Journal of Catalysis **201,** 169–182 (2001)
doi:10.1006/jcat.2001.3244, available online at http://www.idealibrary.com on IDEAL®

Adsorption Reactions of Toluene on the (110) Vanadium Antimonate Oxide Surface

B. Irigoyen,* A. Juan,†,[1] S. Larrondo,* and N. Amadeo*

*Laboratorio de Procesos Catalíticos, Departamento de Ingeniería Química, Facultad de Ingeniería, Universidad de Buenos Aires, 1428 Buenos Aires, Argentina; and †Departamento de Física, Universidad Nacional del Sur, Avda. Alem 1253, 8000 Bahía Blanca, Argentina

Received May 3, 2000; revised November 27, 2000; accepted March 23, 2001

The adsorption reactions of toluene on the (110)-$VSbO_4$ face are studied using the atom superposition and electron delocalization molecular orbital (ASED-MO) semiempirical calculation method. Different sequences (perpendicular and parallel toluene adsorption on the (110) cluster plane) and surface sites (Sb, V, and O atoms) are explored. The results indicate that an Sb–O center participates in the first H-abstraction during toluene parallel adsorption on the Sb–V site. A reaction mechanism involving twofold coordinated oxygen atoms for toluene selective oxidation to benzaldehyde and a probable route to carbon oxides products are proposed. The most exothermic perpendicular and parallel toluene interactions on the (110) oxide surface are analyzed following the changes in the electronic structure of toluene and $VSbO_4$ surface sites using the YAEHMOP code.

Key Words: **toluene oxidation; benzaldehyde; $VSbO_4$; ASED-MO; LDOS.**

1. INTRODUCTION

The catalytic oxidation of aromatic hydrocarbon involves complex mechanisms resulting in a great variety of products under different reaction conditions (1). The knowledge of the mechanisms involved in this process, which occurs on the oxide's surface, is relevant not only to understanding the reactions but also to characterizing the solid's surface properties.

The oxidation of toluene to benzaldehyde is an important process among the selective conversion of hydrocarbons to chemical products of industrial interest. Many attempts to identify the mechanisms of toluene oxidation on metal oxides or mixed oxide based catalysts have been carried out. Two main reaction pathways were proposed (2, 3):

a. The side chain oxidation, which yields aldehydes and acids without affecting the π-electron system of the aromatic ring.

b. The more severe electrophilic oxidation involving destruction of the aromatic nucleus to form anhydrides and carbon oxides.

These reaction mechanisms were confirmed from semiempirical studies of toluene interactions with V_2O_5 (4–6). The authors found that toluene adsorption with the aromatic ring parallel to the cluster plane is the most exothermic process. However, it results in the destruction of the molecule and the formation of carbon deposits or total oxidation products. Perpendicular end-on adsorption of toluene on oxygen sites leads to abstraction of two H-atoms from the methyl group and an adsorbed complex through a strong C–O bond. This complex is considered to be the benzaldehyde precursor. Concomitantly, the V–O–V bonds are dramatically weakened, facilitating desorption of the product.

Moreover, experimental studies led to the conclusion that toluene partial oxidation reactions start with the adsorption of the molecule on the catalyst and abstraction of an H-atom from the methyl group to form an intermediate species (1, 3, 7–10). This may be either desorbed as aldehyde, acid, or further oxidized to carbon oxides.

Although the catalysts based on V_2O_5 have been the most studied for toluene partial oxidation, during recent years V–Sb oxides have received attention because of their catalytic properties for hydrocarbons amm(oxidation) reactions (11–14). Particularly, the experimental results obtained in our laboratory show a selectivity to benzaldehyde of approximately 30% for the oxidation reactions of toluene with $VSbO_4$ catalyst (15). Moreover, in a catalyst based on V_2O_5 strongly doped with Sb the formation of a rutile-type $VSbO_4$ phase was reported (16). This phase shows changes of both electronic and structural character. Electronically, the addition of Sb cations lowers the oxidation state of V, while structurally the Sb interposes between V–O–V chains and helps to isolate each V–O moieties. As a result a more selective catalyst is obtained (16, 17).

The $VSbO_4$ synthesis was initially reported by Birchall and Sleight, who observed a tetragonal structure of rutile-type (18). In this structure, the Sb and V ions are

[1] To whom correspondence should be addressed. E-mail: cajuan@criba.edu.ar.

0021-9517/01 $35.00

present as Sb^{5+} and V^{3+}. The structural characteristics of the vanadium antimony rutile phase depend on the Sb : V ratio (19, 20). For a Sb : V = 1 ratio a rutile-type $VSbO_4$ structure, with different metal–oxygen probable combinations, was reported by Hansen *et al.* from powder diffraction studies (21). They concluded that this oxide shows a cation deficient rutile phase giving place to the formation of coordinatively unsaturated oxygen species. In the same study a bond valence analysis suggested that $OSb_2\square$, $OSbV\square$, and $OV_2\square$ are the most favorable arrangements (the square $\square$ denotes cation vacancies). On the other hand for $FeSbO_4$, a catalyst isostructural with $VSbO_4$, a trirutile structure was reported from electron diffraction studies (22, 23). Thus, the study of the $VSbO_4$ oxide appears to be very complex since the problem of its actual structure as well as the different active sites exhibited on its surface remains as an open question which needs to be clarified.

In the present work, the oxide is modeled following the ideas of Hansen *et al.* (21). To represent the most probable Sb–V combinations reported by these authors, a tetragonal like-trirutile superstructure is used. Moreover, taking into account the results of toluene oxidation on V-oxide reported by Haber *et al.*, our theoretical study involves two main types of toluene interactions with the oxide surface (4). Thus, calculations are carried out for the toluene molecule approaching the cluster along a reaction pathway parallel or perpendicular to the (110)-$VSbO_4$ surface. The semiempirical ASED-MO theory (24) is used to obtain the adiabatic total energies for toluene–oxide interactions. The most exothermic of these are analyzed following the changes in the electronic structure of toluene and $VSbO_4$ surface sites with the YAEHMOP code (25). This method was employed by our group to study the interactions of alcohols and hydrocarbons on different metal oxides surfaces (26–28).

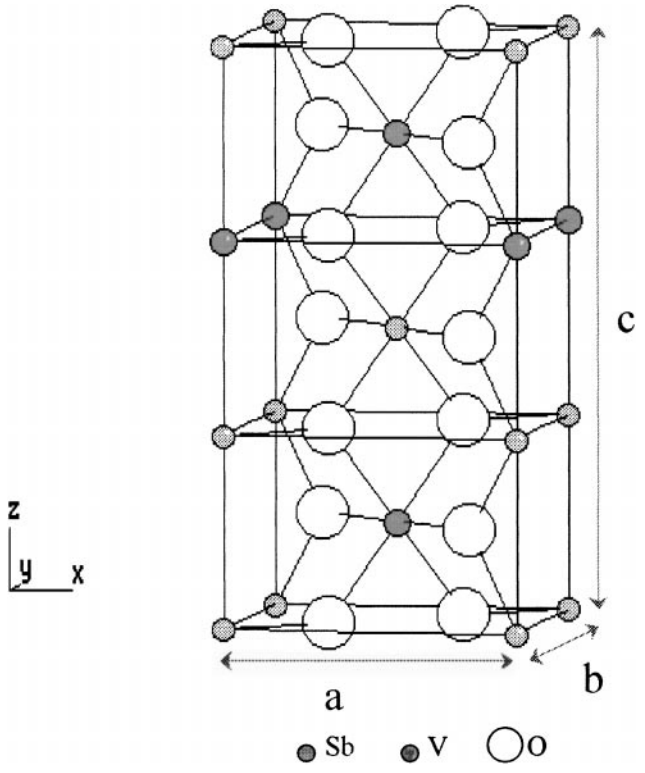

FIG. 1. Tetragonal like-trirutile superstructure of $VSbO_4$.

2. ACTIVE SITES AND ADSORPTION MODEL

A rutile-type tetragonal supercell is used to model the $VSbO_4$ oxide (see Fig. 1). The lattice parameters are: $a = 4.636$ Å, $b = 4.636$ Å, and $c = 9.144$ Å ($= 3 \times 3.048$ Å) (29).

The rutile structure is formed by infinite chains of metal–oxygen octahedra with shared edges and corners. Each metal center bounds to six oxygen atoms (O) while each oxygen bounds to three metal atoms (*M*). The metal–metal distances in the resulting structure of coordination 6 : 3 are always relatively long and there is no effective O...O or *M*...*M* interactions. Additionally, open channels parallel to *z* axis are formed in the crystal.

The (110)-$VSbO_4$ cluster used in our calculations is shown in Fig. 2. It has 228 atoms and a charge of −61. These charge is assigned to ensure that all oxygen anions are in the −2 oxidation state. The (110) plane is chosen because it appears to be one of the most stable crystal face of rutile oxides and results from breaking the smallest number of *M*–O bonds. This surface exhibits an oxygen extra plane and contains the most probable Sb–V combinations reported by Hansen *et al* (21). Moreover many V sites are separated by Sb ions in agreement with the principle of site isolation, an important concept developed by Callahan and Grasselli (30) to improve the selectivity of catalytic oxidation reactions.

The interactions of toluene on the (110)-$VSbO_4$ face are analyzed by performing the calculation of its adsorption energy. To find the energy local minimum the toluene-surface distances, measured from the C-atom of the methyl group to the adsorption site, are optimized varying the *x* and *y* atomic coordinates (in 0.07 Å steps). The calculations are carried out for the experimental geometry of the free toluene and benzaldehyde molecules (31, 32).

The hydrocarbon approaches to the oxide following two main adsorption routes, with the aromatic ring parallel or perpendicular to the catalyst surface. The different active sites explored in these sequences are O, Sb, and V ions; named as S1, S2, and S3, respectively. These sites are indicated in Fig. 3.

In contrast, in the parallel adsorption sequences the phenyl and methyl groups can interact with different sites. Among them, the studied alternatives are enumerated in Table 1.

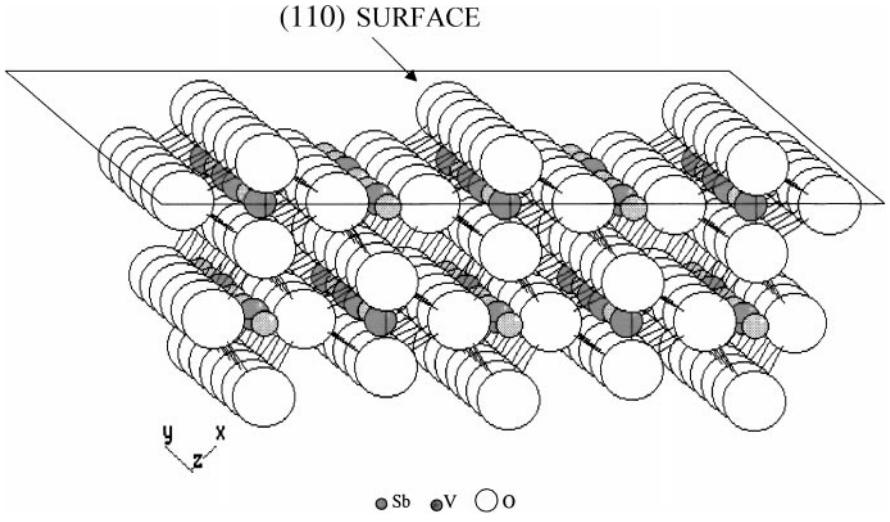

FIG. 2. Cluster $V_{30}Sb_{35}O_{163}$ used in our calculations.

Calculations details are given in the Appendix.

3. RESULTS AND DISCUSSION

The different adsorption sequences and dehydrogenation and oxidation reactions analyzed in this work will be described in the following sections.

3.1. Toluene Perpendicular Adsorption on the (110)-$VSbO_4$ Surface

In the perpendicular adsorption reactions the toluene molecule, with its ring plane normal to the cluster surface (see the insert in Fig. 4), is approximated to the different active sites S1, S2, and S3.

The energy curves for these toluene interactions on S1 (O-atom) and S2 (Sb-atom) sites exhibit long tails with valleys of about −0.2 eV, while C–S1 and C–S2 distances are relatively large (∼2.8 Å) (see Fig. 4). We can infer from these values that toluene perpendicular end-on adsorptions on O and Sb ions are of a physical nature.

On the other hand, the interaction over a S3 site (V-atom) is more favorable and the system reaches a total energy value of −1.78 eV at a C–S3 distance of 2.11 Å (see Fig. 4). The S3 site becomes oxidized and also the methyl group ($[CH_3]^{+0.16}$).

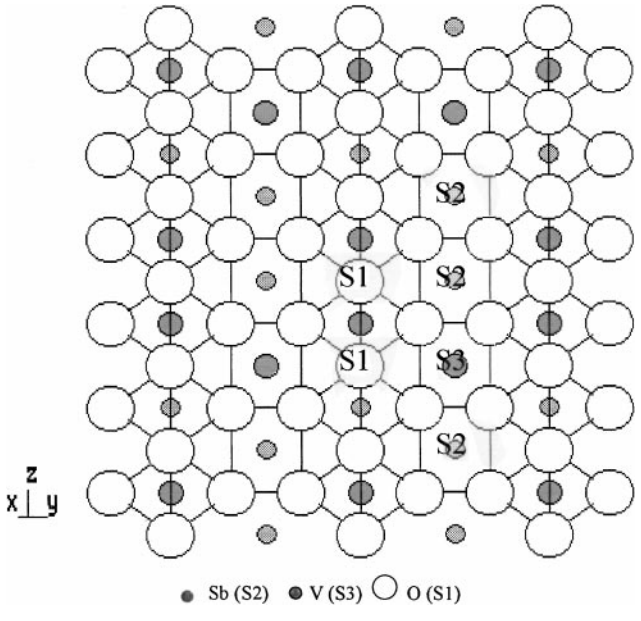

FIG. 3. Catalytic sites on the (110) surface of $VSbO_4$.

3.2. Toluene Parallel Adsorption on the (110)-$VSbO_4$ Surface

In the parallel adsorption reactions the toluene molecule, with its aromatic ring plane parallel to the cluster surface, is approximated to the cluster surface along the *z* axis (see the insert in Fig. 5).

Looking at the energy curves in Fig. 5 we appreciate that the energy valley corresponding to toluene adsorption on A1 sites (O–O) is −0.26 eV, suggesting a physisorptive interaction.

TABLE 1

Different Alternatives for Toluene Parallel Interactions on the (110) Surface of VSbO4

Alternative	Methyl group on	Phenyl group on
A1	S1 (O)	S1 (O)
A2	S2 (Sb)	S2 (Sb)
A3	S3 (V)	S2 (Sb)
A4	S2 (Sb)	S3 (V)

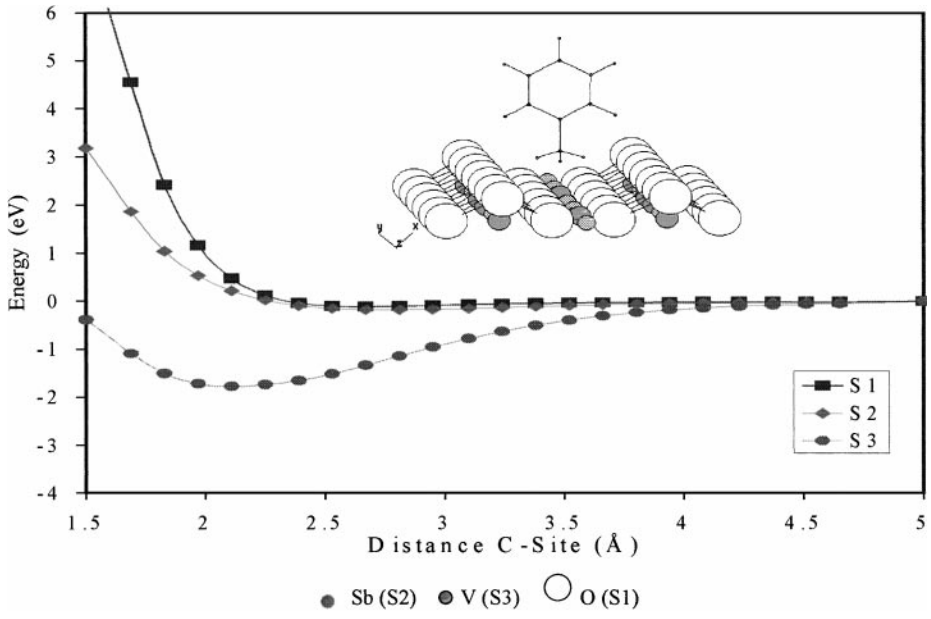

FIG. 4. Perpendicular interactions of toluene on the (110) surface of $VSbO_4$.

A different situation occurs during the reaction over A2 sites (Sb–Sb). When the C atom of the methyl group is placed at a distance of 2.53 Å from Sb a minimum energy value of −1.49 eV is reached. The system shows a weak bond between C and Sb (OP(C–Sb) = 0.12). The optimum value of the total energy curve for toluene–surface interaction A3 (V–Sb) is similar to that of A2 ($\Delta E_{\text{total}} = -2.01$ eV, see Fig. 5). In this case the V cation oxidizes loosing 0.26 e^-.

The total energy curve corresponding to alternative A4 (Sb–V) exhibits a minimum value of −3.22 eV for a C–Sb distance of 2.39 Å. This toluene–surface interaction, with the methyl group placed over a Sb cation and the aromatic ring centered on a V, is the most exothermic among the studied parallel adsorptions. The V cation is strongly oxidized by the loss of 1.78 e^-, while the CH_3 charge is +0.31, almost twice than in the perpendicular case.

The C–Sb interaction developed during the alternative A4 results in slight bonding (OP(C–Sb) = 0.16), while those corresponding to V with the C atoms of the phenyl group are of nonbonding character. In the toluene molecule, all

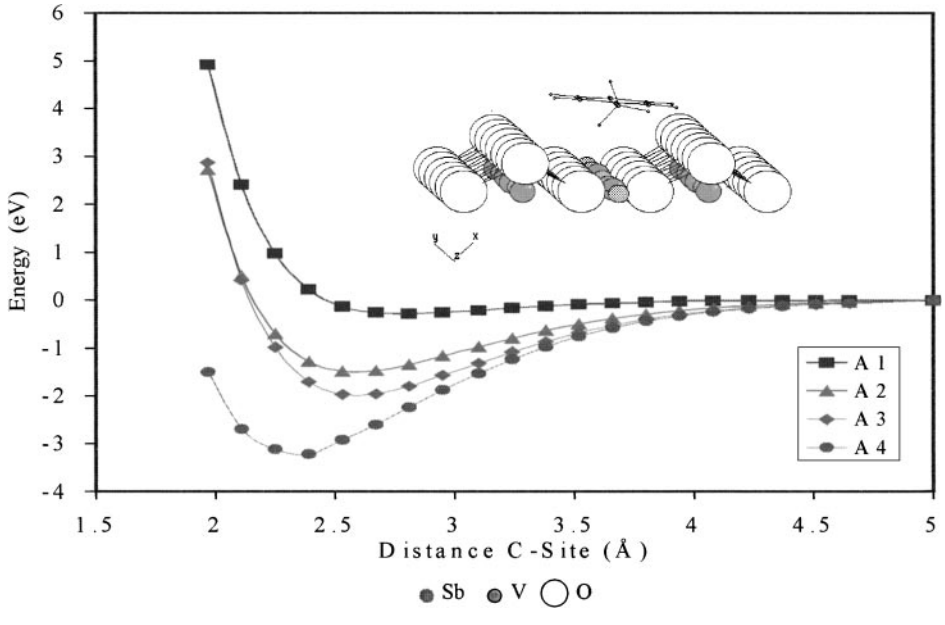

FIG. 5. Parallel interactions of toluene on the (110) surface of $VSbO_4$: A1, O–O; A2, Sb–Sb; A3, V–Sb; A4, Sb–V.

C–H bonds of the aromatic ring become reinforced (∼4%). In addition, the weakening of C–H bonds in the CH_3 group is observed. The greater of these (∼18%) is accompanied by the beginning of an hydrogen bonding interaction with the Sb cation site (OP ∼ 0.2).

These calculations suggest that Sb plays an important role during the first step of toluene oxidation mechanism.

In the well-established area of selective o-xylene oxidation to phtalic anhydride, the catalysts are still based on vanadium oxides strongly doped, particularly, with elements such as Sb, Nb, and Cs (16). In addition, the formation of $VSbO_4$ as one of the phases is postulated to result in a more selective catalyst.

In $VSbO_4$ rutile-type structure, synthesized by solid state reaction of vanadium(V)-oxide and antimony(III)-oxide, the Sb and V ions are present as Sb^{5+} and V^{3+} (18, 33). Hence, a question emerges: are the Sb effects electronic or structural? Both effects were ascribed to Sb: electronically it lowers the oxidation state of vanadium while structurally helps to separate vanadium sites in the surface (13, 16).

To improve our comprehension of antimony role during toluene selective oxidation, all Sb cations on the $VSbO_4$-(110) model surface were replaced by V cations and the perpendicular and parallel interactions computed. During toluene perpendicular approach, the system reaches an energy value of −2.1 eV, while during parallel approach it reaches −5.59 eV. Thus, parallel adsorption on V–V sites results in 2.37 eV more exothermic energy than the computed energy on A4 (Sb–V) sites. Moreover, the strong interactions of carbon atoms with surface V and O atoms are in agreement with the results reported by Haber *et al.* (4). These authors found that toluene parallel adsorption on V_2O_5 involves deep oxidation of the carbon skeleton, resulting in the formation of carbon deposits or total oxidation products.

Our calculations show that the interactions of hydrogen atoms from the methyl group with V cation sites are of antibonding character while during A4 an hydrogen interaction of bonding character with the Sb-cation site is observed. This suggests that Sb plays an important role in the hydrogen abstraction. In addition, the participation of Sb sites (specifically Sb^{3+} sites) on vanadium–antimony oxide surfaces is postulated by Grasselli to be responsible for the activation and α–H abstraction of propylene (16).

3.3. Toluene Dehydrogenation on the (110)-$VSbO_4$ Surface

The mentioned result in the preceding paragraph regarding the greater weakening of a C–H bond in the CH_3 (alternative A4: $\Delta E_{\text{total}} = -3.22$ eV) is taken as the starting point for the dehydrogenation mechanism. Although the overlap populations between the H atom and its neighboring O atoms are not significant, an hydrogen interaction of bonding character with the Sb cation site is observed (OP ∼ 0.2). This one is favored by the electron donation from CH_3 (∼0.3 e^-) to Sb; which in addition debilitates its C–H bonds.

In order to compare the hydrogen transfer to an Sb–O center with that to other O sites, the H abstractions from the methyl group to the Sb–O center (see Fig. 6a, left) and the nearest O sites (see Fig. 6a, right) are studied. The V sites are not considered due to their unfavorable geometric position. Moreover, we found no theoretical evidence of hydrogen bonding with them.

Considering the approach to an O site we can see that hydrogen, after overcoming a barrier of 3.02 eV (see Fig. 6b, reaction step 1), bonds to oxygen at a distance of 1.1 Å with an OP(H–O) = 0.49. The system reaches a stable configuration with $\Delta E_{\text{total}} = -1.08$ eV. On the other hand, if hydrogen approaches the Sb–O center the system reaches a final state of $\Delta E_{\text{total}} = -4.42$ eV, which is 3.34 eV more stable than the former case (see Fig. 6b, reaction step 2). The hydrogen is at 1.19 Å from the Sb cation and the bonding character of this interaction raises to 0.74.

In a recent paper Grzybowska-Swierkosz mentioned that the couple Me^{n+}–O^{2-} is often considered as an active center for the activation of a C–H bond (34). Two possibilities can be envisaged assuming heterolytic splitting on such a couple:

(a) Formation of a proton and a carboanion which by donation of electrons to a cation is transformed into a carbocation.

(b) Abstraction of a hydride ion with the formation of a Me^{n+}–H bond and a carbocation (35–38).

Weber found that during the oxidative dehydrogenation of methanol on metal oxides (V-substituted Keggin anions) the stereochemically plausible, suprafacial pathway would involve transfer of the hydrogen to the reducible transition-metal cation (39). Also, Oyama *et al.* showed that participation of the metal-cation in the transfer of hydrogen from an alkoxy or alkyl ligand is thermodynamically plausible (40).

Our calculations show that hydrogen develops bonding interactions with the Sb–O center and the O sites, being that it is more exothermic with the Sb–O center than with other O sites. There is important evidence in the literature that Sb–O–H moieties are the first formed species of α-H transfer to the V–Sb–oxide surface (16, 17). Thus, the difference in the adsorption energy of both interactions might be considered as an indication that O sites and Sb–O centers could compete during toluene dehydrogenation to end with H-abstraction on the Sb–O center.

Taking into account our calculations, in the study of the dehydrogenation of toluene after adsorption alternative A4 two mechanisms for C–H bond breakage on Sb–O centers are considered: sequential and simultaneous (see Figs. 7a and 7b). The total energy curves of these reactions can be seen in Fig. 8. The value $\Delta E_{\text{total}} = 0$ eV corresponds to the system "cluster + toluene in the vacuum" (reaction step 0), while the value $\Delta E_{\text{total}} = -3.22$ eV corresponds

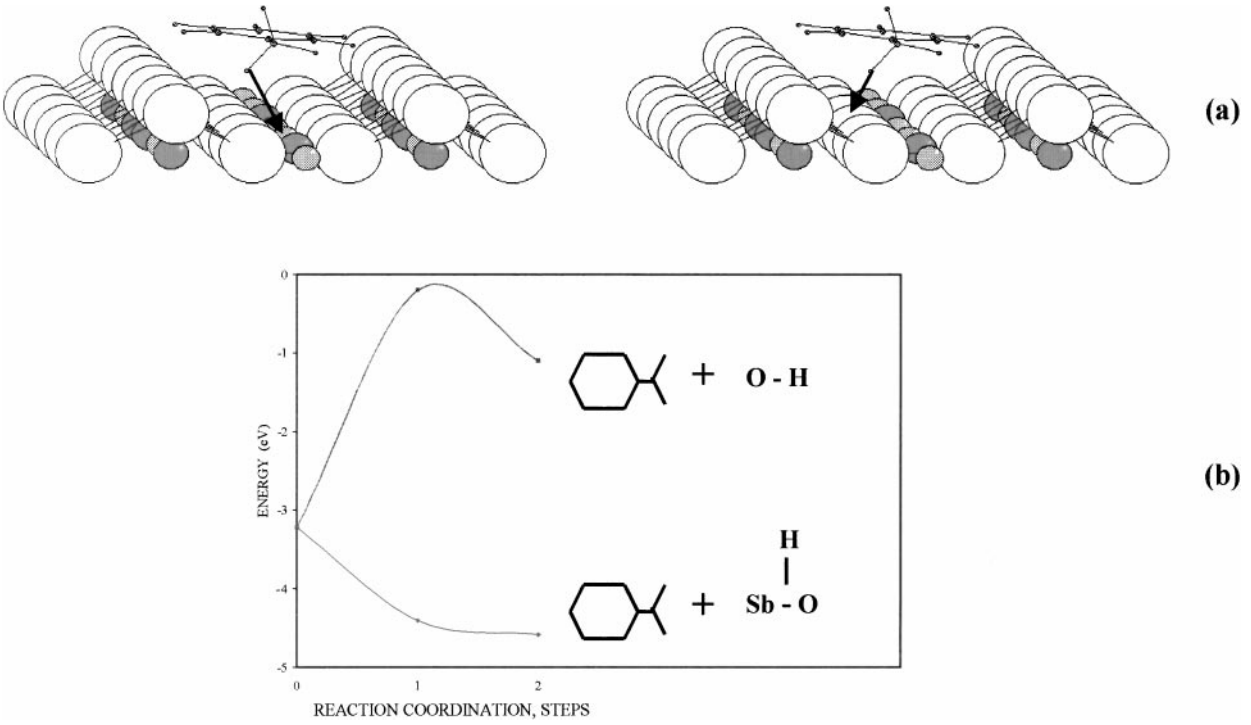

FIG. 6. Different alternatives explored for the initial dehydrogenation of toluene on the (110) surface of $VSbO_4$. (a) left, H-abstraction on Sb–O center; right, H-abstraction on O site. (b) Energy curves for these alternatives.

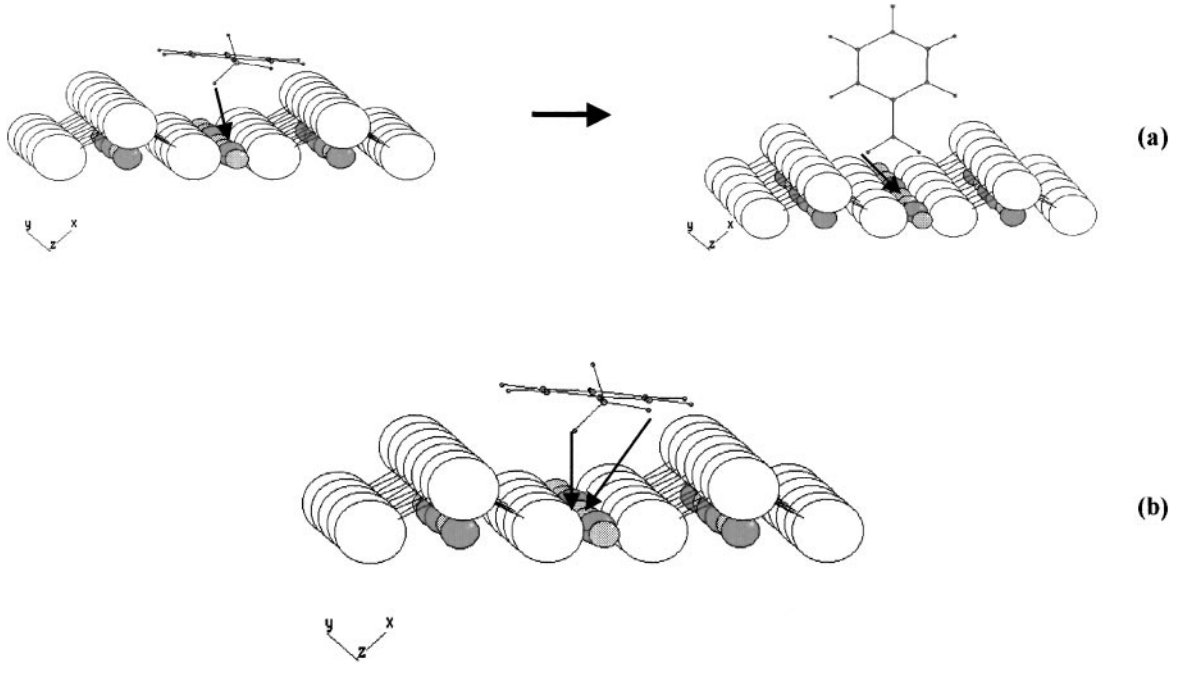

FIG. 7. Dehydrogenation of toluene on Sb–O centers. (a) Sequential dehydrogenation of toluene: left, first H-abstraction; right, second H-abstraction. (b) Simultaneous dehydrogenation of toluene.

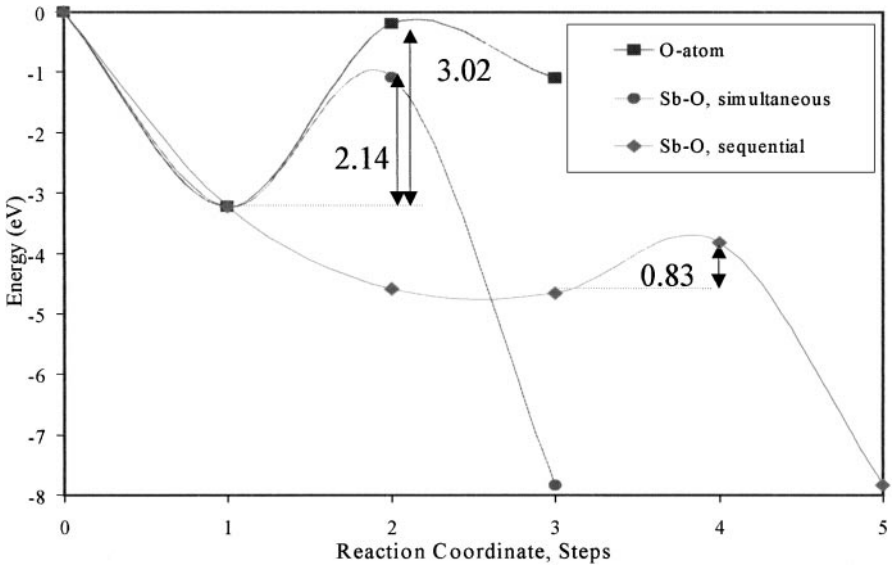

FIG. 8. Different alternatives explored for the dehydrogenation of toluene on the (110) surface of $VSbO_4$. Step 0: Cluster + toluene in the vacuum; Step 1: Optimum energy value of toluene parallel adsorption A4 (Sb-V). *Dehydrogenation curve on O-atom*: Step 2: Energy barrier through the first H-abstraction after toluene parallel adsorption A4; Step 3: Final state after the first H-abstraction on O-atom. *Simultaneous dehydrogenation curve on Sb–O centers*: Step 2: Energy barrier through the two H-abstractions after toluene parallel adsorption A4; Step 3: Final state after the two simultaneous H-abstractions. *Sequential dehydrogenation curve on Sb–O centers*: Step 2: Final state after the first H-abstraction after toluene parallel adsorption A4; Step 3: Optimum energy value of H_5C_6–CH_2 perpendicular adsorption on Sb-cation site; Step 4: Energy barrier through the second H-abstraction after H_5C_6–CH_2 perpendicular adsorption on Sb-cation site; Step 5: Final state after the two sequential H-abstractions.

to the optimum energy value of interaction A4 (reaction step 1).

3.3.1. Sequential dehydrogenation over Sb–O centers. The sequential dehydrogenation of toluene, shown in Fig.7a, involves two H-abstractions. During the first,

$$H_5C_6 - CH_3 + (Sb{-}O) \rightarrow H_5C_6 - CH_2 + (Sb{-}\overset{H}{O}), \qquad [1]$$

the weak C–H bond is stretched to send one hydrogen toward an Sb–O center. Finally, the C–H bond breaks and the remaining H-atoms of CH_2 become planar with the aromatic ring taking an angle $\langle HCC_{phenyl}\rangle = 120^\circ$. All C–H and C–C bonds reinforce making possible the H_5C_6–CH_2 desorption (Fig. 8, reaction step 2: $\Delta E_{total} = -4.58$ eV). This planar geometry has been described as one of the most stable for benzyl radical (32). Our results show that the C–H bond breaking occurs without energetic barrier, suggesting that the first H-abstraction is a very fast process. Moreover, the H_5C_6–CH_2 can easily leave this place (the desorption energy is ∼0.01 eV), travel along the catalytic surface, and react on other sites. It is also possible that reorientation of H_5C_6–CH_2 to the surface occurs. If we continue with the parallel orientation, the system undergoes to total oxidation products (see also Section 3.4).

On the other hand if a perpendicular reorientation of H_5C_6–CH_2 is performed on the (110)-$VSbO_4$ surface this molecular fragment can interact with three different sites (analogous to S1, S2, and S3 sites in toluene perpendicular adsorption). When the H_5C_6–CH_2 is approximated to S1 (O-atom) or S2 (Sb-atom) sites the energy of the system decreases only by 0.07 eV at a C-site distance of ∼2.8 Å. Nevertheless, the weakness of a C–H bond in the CH_2 group (∼4%) and the starting of an hydrogen bonding interaction with the Sb–O center is appreciated only through the interaction on S2 site (OP ∼ 0.02). If the adsorption occurs on S3 (V-atom), an interaction of bonding character is developed. The optimum energy value of −7.63 eV is reached at a C–S3 distance of 1.55 Å (OP(C–V) ∼ 0.62).

The overlap population analysis, performed for the perpendicular adsorption of H_5C_6–CH_2 on the three different sites of the catalyst surface, shows the weakening of one of its lateral chain C–H bonds (∼4%). This bond is debilitated during the H_5C_6–CH_2 reaction on the S2 site (Fig. 8, reaction step 3: $\Delta E_{total} = -4.65$ eV), suggesting that the second C–H bond can be broken on the mentioned Sb–O center:

$$H_5C_6 - CH_2 + (Sb{-}O) \rightarrow H_5C_6 - CH + (Sb{-}\overset{H}{O}). \qquad [2]$$

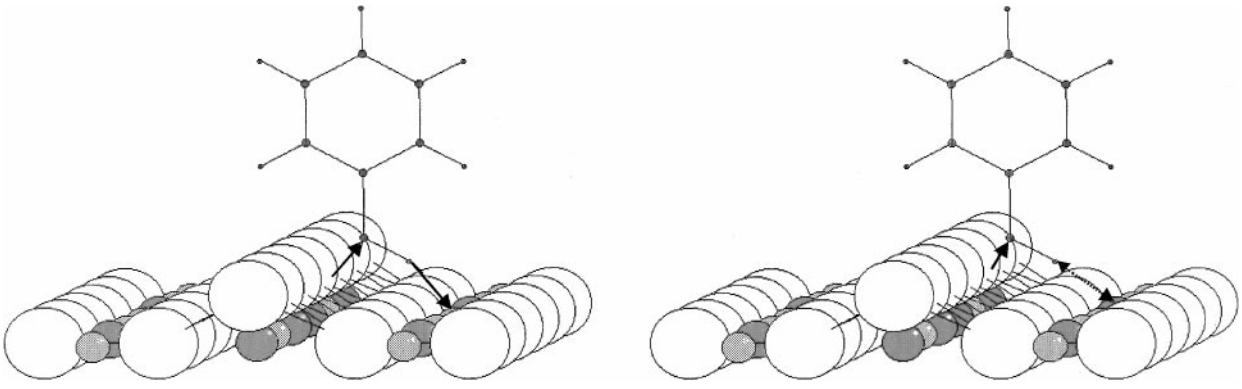

FIG. 9. Schematic approach of H_5C_6–CH species to O-atoms of the surface extra plane: left, Hydrogen faces Sb-cation; right, Hydrogen faces V-cation.

After overcoming an energy barrier of 0.83 eV height (Fig. 8, reaction step 4) the H-atom finally bonds to Sb–O center at a distance of 1.25 Å while an energy minimum of −7.83 eV is reached (Fig. 8, reaction step 5).

3.3.2. Simultaneous dehydrogenation over Sb–O centers. In the simultaneous mechanism of toluene dehydrogenation both hydrogen atoms are concomitantly transferred to each nearest Sb–O center (see Fig. 7b).

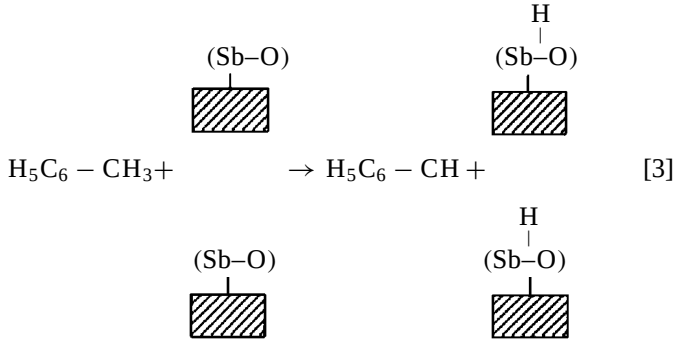

In Fig. 8, reaction step 2, it can be seen that the energy barrier height is 2.14 eV. The unfavorable geometric position of one of the H atoms to the respective Sb–O center can be one of the reasons for this high activation energy. At the end, the remaining C–H fragment rearranges to give the H_5C_6–CH planar species.

The comparison of the studied mechanisms for toluene dehydrogenation shows that the sequential hydrogen abstraction is preferred.

3.4. Formation of Oxygenated Products on the (110)-$VSbO_4$ Surface

The H_5C_6–CH species formed during the sequential dehydrogenation of toluene ($\Delta E_{total} = -7.83$ eV) can be easily desorbed without any significant change in the energy of the system. So, the molecular fragment is approximated in a perpendicular way (see Section 3.3.1) to the O atoms of the surface extra oxygen plane. Two possibilities are considered as the hydrogen of the CH group faces different sites: H faces an Sb cation (see Fig. 9, left) or a V cation (see Fig 9, right).

When the H of the H_5C_6–CH species faces an Sb cation, two bonds are established by C and H atoms of its lateral chain: C–O (OP ∼ 0.90) and H with Sb–O center (OP ∼ 0.23). In addition, the HC–C_{phenyl} bond appears debilitated (∼5%). Subsequently, this union is broken leading to the phenyl desorption. At the same time the hydrogen is approximated to the Sb–O center until a strong bond of 1.25 Å length is established (OP ∼ 0.56) and the system reaches its optimum energy value ($\Delta E_{total} = -8.95$ eV). At the end, while carbon monoxide is desorbed the total energy rises to −6.57 eV.

Nevertheless, when the H of the former species faces vanadium, an H–V interaction of nonbonding character is observed. Therefore a C–O bond begins to appear (OP(C–O) = 0.90) accomplished by the reinforcing of the HC–C_{phenyl} bond. This situation indicates the formation of a possible aldehyde precursor ($\Delta E_{total} = -8.00$ eV). If this procedure is allowed, desorption of benzaldehyde increases the energy of the system to −4.32 eV.

The participation of O twofold coordinated in the reactions toward oxygenated products is in agreement with the proposal of Nilsson *et al.*, who assigned an important mechanistic role to this kind of oxygen atoms (13). Moreover, the beginning of a C–O link during benzaldehyde and CO formation is accomplished by the respective O–metal bond destabilization in the solid.

Subsequent desorption of these products leaves an oxygen vacancy on the oxide surface.

3.5. Formation of Total Oxidation Products on the (110)-$VSbO_4$ Surface

The H_5C_6–CH_2 can also approach the active sites of the catalytic surface in a parallel way similar to that described

for toluene (see Section 3.2), giving place to a many different reactions. During the interaction over O atoms (like-A1) the adsorption energy decreases by only 0.27 eV at a C–O distance of 2.53 Å, indicating that this reaction is of physical nature. Nevertheless, when this fragment approaches to Sb sites (reaction like-A2) the C-atom of CH_2 group establishes a C–Sb bond of 2.40 Å length (OP(C–Sb) $\sim$ 0.42) with an energy value of $\Delta E_{total} = -7.54$ eV. Also in the approximation like-A3 that C-atom bonds to the corresponding V site (OP(C–V) = 0.23), but this interaction is less exothermic ($\Delta E_{total} = -6.72$ eV) than the previous interaction (like-A2).

In contrast, the energy of the system reaches its minimum value ($\Delta E_{total} = -9.75$ eV) when the CH_2 group lies over antimony and the ring nucleus over vanadium (like-A4) at the C–Sb distance of 2.25 Å (OP(C–Sb) = 0.48). Due to the strong adsorption of H_5C_6–CH_2 on these catalyst sites the interaction might result in the fragmentation of the adsorbed species, the formation of total oxidation products, and finally the deposit of carbon.

The main sequences of formation of products during toluene approximation to (110)-$VSbO_4$ surface are schematized in Fig. 10. The comparison of the energy values corresponding to the oxygenated products shows that benzaldehyde formation is a likely alternative. Nevertheless, parallel adsorption of the H_5C_6–CH_2 species, resulting in the formation of carbon oxides or the deposit of coke, is energetically more favorable. This result is in agreement with our experimental observation of limited benzaldehyde selectivity of about 30% for toluene partial oxidation on the $VSbO_4$ catalyst (15).

3.6. Electronic Structure: A Preliminary Analysis

A preliminary electronic analysis of the most exothermic parallel A4 and perpendicular S3 toluene interactions on the (110)-$VSbO_4$ surface is presented.

The total DOS of toluene, toluene + $VSbO_4$ system after parallel adsorption A4 (Sb–V), and $VSbO_4$ cluster are shown in Fig. 11. In Fig. 11a, it can be seen that the energy levels of an isolated toluene are narrow (the organic molecules are considered far away from each other). On the other hand, in Fig. 11c, the total DOS of the (110)-$VSbO_4$ cluster by itself is shown. It resembles that of 3D solids with rutile structure as RuO_2, OsO_2, IrO_2, and TiO_2 (41–43). However, our hypothetical structure is trirutile and we are limited to a cluster.

TiO_2 is wide band gap ($\sim$3.05 eV) semiconductor and this property is well described in DOS calculations. Other transition metal dioxide compounds with rutile-like structures show different behavior. Among them, VO_2 is an example of metals or semimetals (41). Thus, the presence of vanadium in our oxide might be the reason for the small peaks which appear above the Fermi level in the cluster total DOS ($E_F = -10.26$ eV, see Fig. 11c). Moreover, Burdett and Hughbanks reported that intermediate structures between rutile and that of octahedral layered compounds like $RuO_2{}^{-0.33}$ (in hollandite system $BaRu_6O_{12}$) are

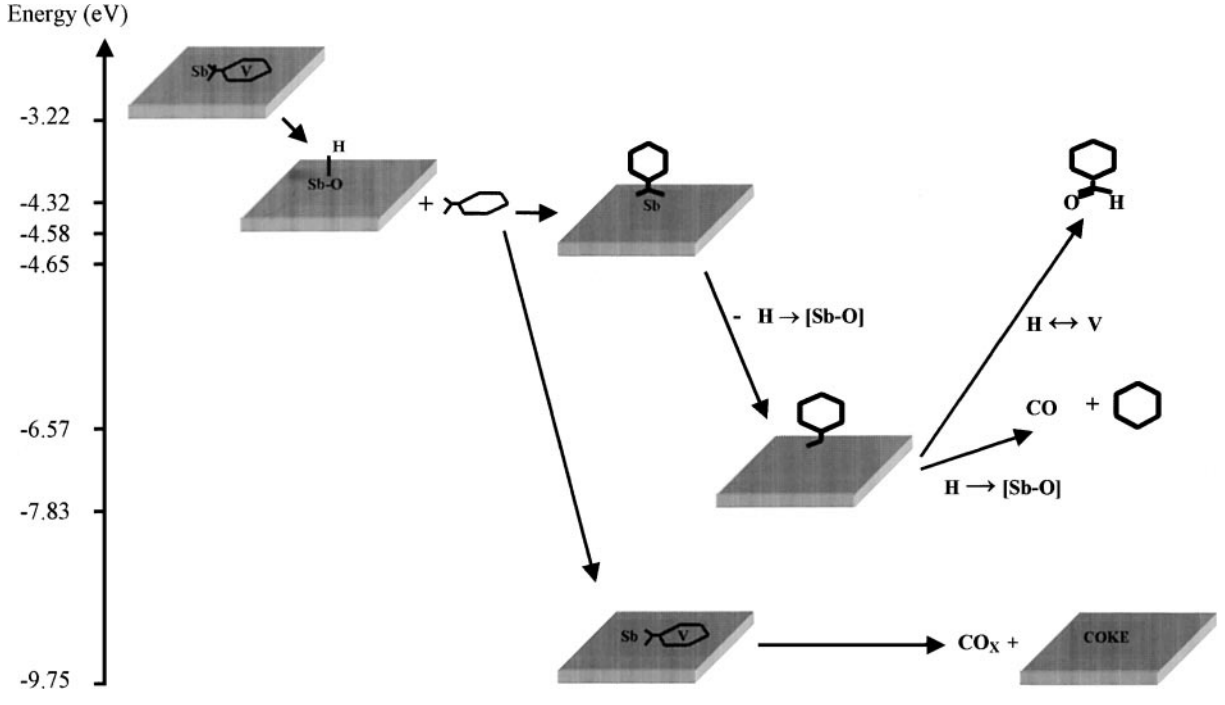

FIG. 10. Schematic formation of toluene products.

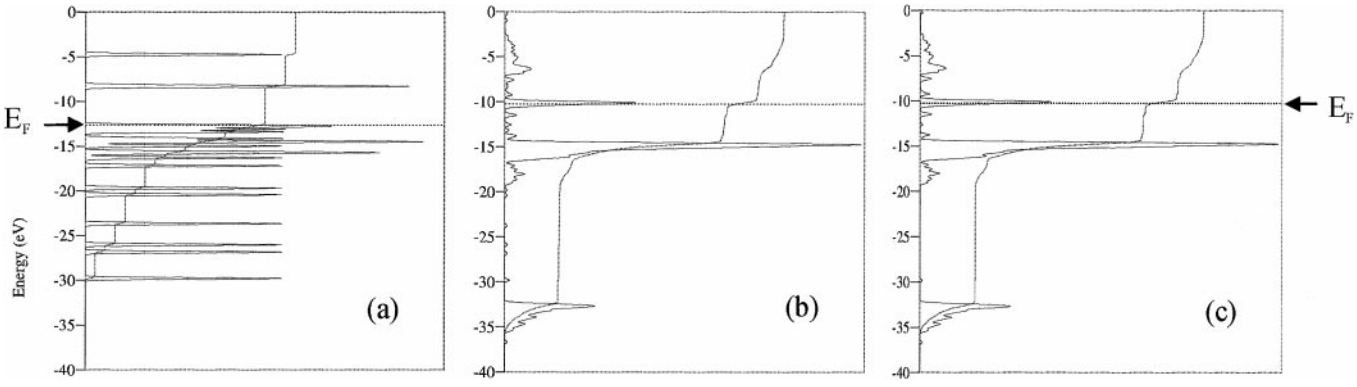

FIG. 11. The DOS of toluene, $VSbO_4$ cluster, and their composite system: (a) total DOS of free toluene; (b) LDOS of toluene on the $VSbO_4$ surface after toluene parallel adsorption A4; (c) total DOS of the $VSbO_4$ cluster.

present above the oxide *p* bands and near the Fermi level (44). The origin of those small bands above −10.26 eV could be somewhat similar.

In the rutile TiO_2 structure, there are infinite chains of edge-sharing MO_6 octahedral (*M*: metal) running in one direction in the crystal but the metal–metal separations are always relatively long (44, 45). Then, taking into account that our hypothetical $VSbO_4$ structure is rutile-like and oxygen has quite distinct 2*s* and 2*p* levels, we may expect no effective O—O, V—V, or Sb—Sb interactions. The shortest O–O, V–V, Sb–Sb, and V–Sb distances are substantial (2.43, 3.62, 3.05, and 3.05 Å, respectively). Thus, no metal–metal interactions are present and the localized octahedral bonding is maintained.

The cluster DOS (see Fig. 11c) presents well-separated O_{2s}, O_{2p}, V, and Sb bands. The top of the band at −32 eV is mainly O_{2s} bonding orbitals, while the bottom is Sb_{5s}. In this energy region, the V_{3d} (t_{2g}) contribution is quite small. Between −19.4 and −16.7 eV the small band is due to Sb_{5p} orbitals. Next to −14.8 eV there are contributions mainly from O_{2p} (O–metal bonds) and a small contribution from V_{3d} and Sb_{5p}. The O_{2p} orbitals segregate into $O_{p\sigma}$ orbitals, whose density lobes point toward the metals and $O_{p\pi}$, whose lobes point perpendicular to them. Most of those orbitals are bonding between the O_{2p} (>80%) and the V_{3d} bands (<20%), similar to that reported by Grunes *et al.* for TiO_2 (42). The peak at −10.1 eV corresponds to V_{3d} (t_{2g}) orbitals. Higher in energy above the Fermi level are the V_{3d} (e_g) metal orbitals, which are antibonding with the oxygen. The V_{4s} and V_{4p} bands lie much higher in energy and are unoccupied. Mattheiss reports very similar electronic structure calculations (LCAO-APW) in several transition metal dioxides with rutile structure: RuO_2, OsO_2, and IrO_2 (41). Most of the width of the antibonding *d* band arises from the covalent overlap interactions of the transition metal with the O_{2s} and O_{2p} orbitals (41). Regarding the other metals forming our cluster, it seems that no effective V–Sb interactions are present.

Some of the preceding analysis is based on bulk considerations of the solid; however, from photoemision experiments (46) and theoretical calculations (47) the electronic structure of the defective free rutile surface is essentially indistinguishable from that of the bulk, whatever the topology of the surface.

We move now to a summary description of the electronic structure of the adsorbate before and after its interaction with the oxide surface and the modification of this surface in two selected adsorption cases, the parallel A4 and the perpendicular S3.

The toluene DOS in Fig. 11a presents several peaks coming from the interaction of the aromatic ring with the methyl fragment (−26.7, −26, and −23.6 eV). Next to −20 eV and at −17.2 eV and −16.3 eV the peaks come mainly from the phenyl group. Next to −15 eV there are also methyl–phenyl interactions. In this last region, the main changes may be produced when the adsorbate interacts with the oxide surface. Although the C_{methyl}–C_{phenyl} bond is strong with respect to reduction, if some electronic density is removed (oxidation) it weakens.

The oxidation of toluene could weaken the π system of the phenyl ring, decreasing its overlap population in about 50%. In addition, the overlap population of the σ bonds in the ring also diminishes but it is less affected.

Figure 11b shows the total DOS of the composite (110)-$VSbO_4$ + toluene system after the toluene parallel adsorption A4. As it can be seen, no extended effects are present and the interaction seems to be local. A detailed discussion about this interaction is performed in the next paragraph.

The projected DOS of the catalytic sites involved in the toluene parallel adsorption A4 (Sb–V) are shown in Fig. 12. Looking at the Sb atomic projection before and after its interaction with the methyl group (see Figs. 12a and 12b), a strong decrease in its electronic density at −7.6 eV can be seen. This region matches in energy to that of a toluene unoccupied orbital which band is broaden after this adsorption. In addition, some Sb states are pushed to −1 eV

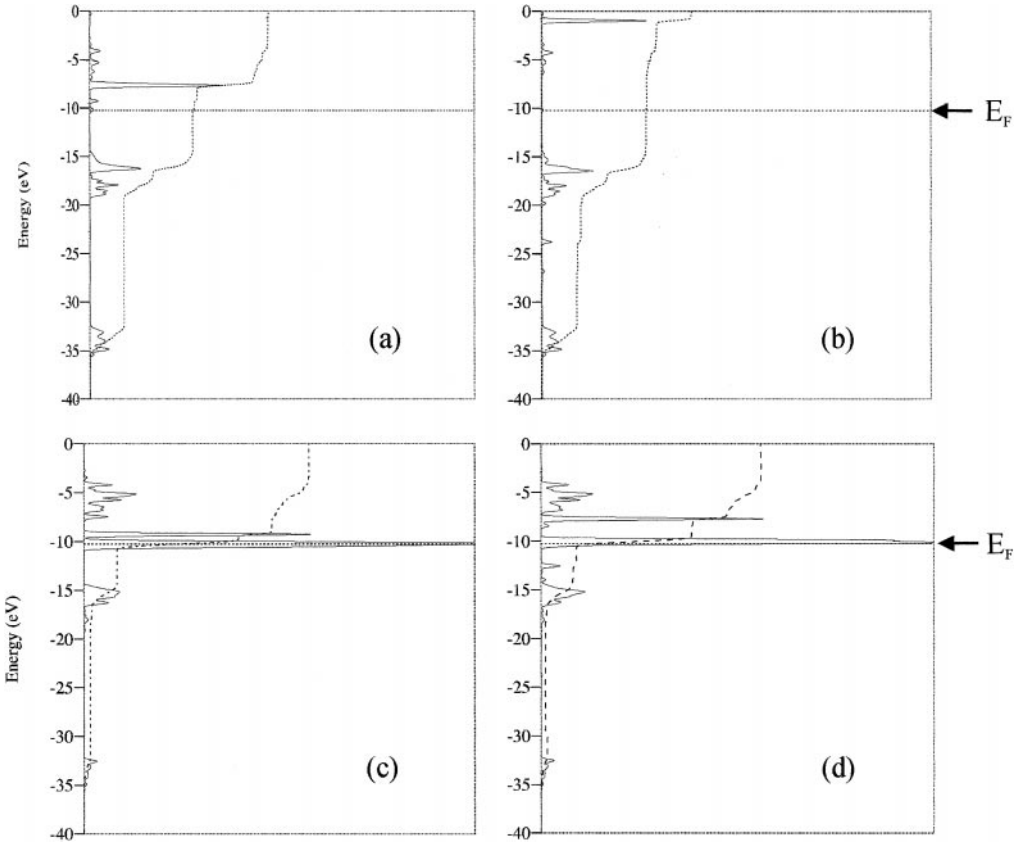

FIG. 12. The LDOS of the Sb and V atoms on the bare $VSbO_4$ cluster and after toluene parallel adsorption A4 (methyl group on Sb and phenyl group on V): (a) LDOS of Sb on the $VSbO_4$ cluster surface; (b) LDOS of Sb on the $VSbO_4$ cluster surface after toluene interaction A4; (c) LDOS of V on the $VSbO_4$ cluster surface; (d) LDOS of V on the $VSbO_4$ cluster surface after toluene interaction A4.

after methyl interaction on this catalytic site. In contrast, the LDOS of the V atom, before and after its interaction with the phenyl fragment (see Figs. 12c and 12d), shows a decrease at −10 eV. Starting with two sharp peaks, after toluene adsorption only one peak remains. Moreover, the V_{3d} orbital depopulation in that region is in agreement with the vanadium oxidation previously described (see Section 3.2). The small peak at −12.5 eV comes from V interaction with the HOMO of toluene while the band at −7.7 eV comes from that with an unoccupied toluene orbital. The toluene DOS for the parallel adsorption A4 presents significant changes in the (−19, −12 eV) region (see Fig. 13b). These changes are indicative of toluene bonding with the surface sites.

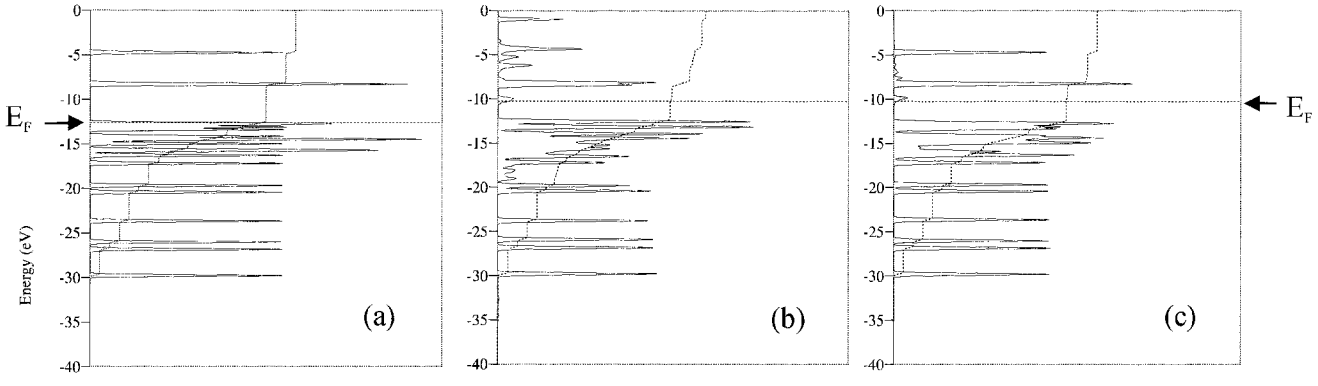

FIG. 13. The DOS of toluene: (a) total DOS of free toluene; (b) LDOS of toluene on the $VSbO_4$ cluster surface after toluene parallel adsorption A4; (c) LDOS of toluene on the $VSbO_4$ cluster surface after toluene perpendicular adsorption S3.

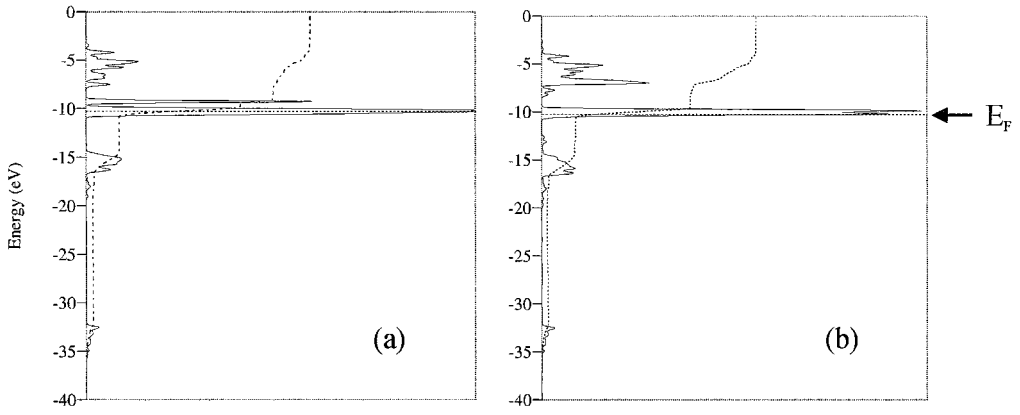

FIG. 14. The LDOS of V on the bare $VSbO_4$ cluster and after toluene perpendicular adsorption S3: (a) LDOS of V on the $VSbO_4$ cluster surface; (b) LDOS of V on the $VSbO_4$ cluster surface after toluene interaction S3.

Regarding toluene perpendicular adsorption S3 (V), it can be seen that the electronic structure of atomic V presents subtle changes before and after this interaction (see Figs. 14a and 14b). The band at −10 eV is somewhat broader likely by a superposition of toluene orbitals. However, the toluene orbitals hybridization in the (−19, −12 eV) region is much lower than that in the parallel adsorption A4 (see Figs. 13c and 13b, respectively).

Further research is required to better understand orbital by orbital modifications after the several discussed toluene interactions on $VSbO_4$ surface sites. This preliminary study could guide us in the near future to shed more light on this catalytic system.

4. CONCLUSIONS

The toluene adsorption reactions on the (110)-$VSbO_4$ face were studied by using the ASED-MO theory. Different sequences of perpendicular and parallel toluene approach to cluster surface were explored.

The calculations suggest a mechanism with two sequences for toluene interactions similar to that proposed for aromatic hydrocarbon oxidation reactions. Besides, the molecule activation is found to be the preliminary step. In this step, during the parallel adsorption of toluene with the methyl group on Sb and the phenyl on V, the first H-abstraction involves the participation of Sb cation.

Once the rupture of the methyl C–H bond occurs, the H_5C_6–CH_2 species was desorbed and its oxidation was studied along two routes. The first route is characterized by the strong parallel adsorption of this intermediate. This route probably leads to the aromatic ring destruction and formation of total oxidation products and carbon deposit. The second route involves oxidation of the side chain to produce benzaldehyde through the H_5C_6–CH_2 perpendicular end-on interaction on Sb sites.

The coke formation, energetically more favorable than the aldehyde production, may explain the difficulties in attaining high selectivity in toluene gas phase oxidation on $VSbO_4$.

The preliminary electronic analysis was restricted to the cluster and the most exothermic perpendicular S3 and parallel A4 toluene interactions on its surface. Although the DOS of the $VSbO_4$ cluster is quite similar to other DOS of solids with rutile-like structures, the Sb also contributes mainly in the region next to −14.8 eV. On the other hand, while for S3 the calculations show a hybridization of those toluene orbitals coming from the methyl fragment, for A4 they come from the methyl–phenyl interactions energy region.

APPENDIX: COMPUTATIONAL DETAILS

The calculations were carried out using the ASED-MO formalism (24), which is a semiempirical method capable of making a reasonable prediction of molecular and electronic structures. The ASED-MO theory is based on a physical model of molecular and solid electronic charge density distribution functions, whereby the last is partitioned into a perfect following (with respect to the nucleus) atom part and an imperfect following bond charge part. This method was described in a previous paper (27). The calculation of the adsorption total energy (ΔE_{total}) is performed as the difference between the total energy of the system when the adsorbed species/molecular fragment are at a finite distance from the surface, and the same energy when those species are far away from the solid surface. That is, the adsorption energy is calculated as

$$\Delta E_{\text{total}} = E(\text{adsorbed species/oxide}) - E(\text{species}) - E(\text{oxide}) + \sum E_{\text{repulsion}}.$$

Here E is the electronic energy. The repulsion energy ($E_{\text{repulsion}}$) of nucleus B in the presence of a fixed atom A is

TABLE 2

Atomic Parameters

Atom	Orbital	IP (eV)	ξ_1	ξ_2	C_1	C_2
C	2*s*	−21.40	1.625			
	2*p*	−11.40	1.625			
H	1*s*	−13.60	1.300			
V	4*s*	−8.81	1.300			
	4*p*	−5.52	1.300			
	3*d*	−11.00	4.750	1.700	0.4755	0.7052
Sb	5*s*	−18.80	2.323			
	5*p*	−11.70	1.999			
O	2*s*	−32.30	2.275			
	2*p*	−14.80	2.275			

calculated from

$$E_{\text{repulsion}} = \frac{1}{2}\sum_{A}\sum_{B\neq A} E_{AB},$$

where E_{AB} is a pairwise electrostatic energy term. The summation is extended over all involved atoms.

The atomic parameters used in this work: ionization potential (IP), Slater exponents (ξ_i), and linear coefficients (c_i), are those reported by Hoffmann *et al.* for O, V, and Sb atoms (48–50). Those of C and H are taken from Minot and Gallezot (51). These parameters are listed in Table 2.

Through this paper, two conceptual tools: DOS and overlap population (OP) are used to better understand toluene-$VSbO_4$ interactions. These analyses were performed by means of the YAEHMOP code (25). The DOS curve is a plot of the number of orbitals per unit volume per unit energy. Looking at the OP, we may analyze the extent to which specific states contribute to a bond between atoms or orbitals (43).

ACKNOWLEDGMENTS

Our work was supported by Universidad de Buenos Aires, Fundación Antorchas, ANPCYT (PICT 12-03576) and Departamento de Física—Universidad Nacional del Sur. Useful suggestions by E. Mershrod were greatly appreciated.

REFERENCES

1. Andersson, S. L. T., *J. Catal.* **98**, 138 (1986).
2. Bielanski, A., and Haber, J., *in* "Oxygen in Catalysis," Vol. 43. Dekker, New York, 1990.
3. Zhu, J., and Andersson, S. L. T., *J. Catal.* **126**, 92 (1990).
4. Haber, J., Tokarz, R., and Witko, M., *in* "New Developments in Selective Oxidation II" (V. Cortés Corberán and S. Vic Vellón, Eds.), p. 739. Elsevier, Amsterdam, 1994.
5. Witko, M., Haber, J., and Tokarz, R., *J. Mol. Catal.* **82**, 457 (1993).
6. Witko, M., Hermann, K., and Tokarz, R., *Catal. Today* **50**, 553 (1999).
7. Bulushev, D. A., Kiwi-Minsker, L., and Renken, A., *Catal. Today* **57**, 231 (2000).
8. Sanati, H., and Andersson, A., *Ind. Eng. Chem. Res.* **30**, 312 (1991).
9. Wojciechowska, M., Lomnicki, S., and Gut, W., *Catal. Lett.* **20**, 305 (1993).
10. Hatayama, F., Ohno, T., Marnoka, T., and Miyata, H., *React. Kinet. Catal. Lett.* **44**(2), 451 (1991); **45**(2), 265 (1991).
11. Guttmann, A. T., Grasselli, R. K., and Brazdil, J. F., U.S. Patents 4784979 (1988) and 4879264 (1989).
12. Centi, G., Foresti, E., and Guarnieri, F., *in* "New Developments in Selective Oxidation II" (V. Cortés Corberán and S. Vic Vellón, Eds.), p. 281. Elsevier, Amsterdam, 1994.
13. Nilsson, R., Lindblad, T., Andersson, A., Song, C., and Hansen, S., *in* "New Developments in Selective Oxidation II" (V. Cortés Corberán and S. Vic Vellón, Eds.), p. 293. Elsevier, Amsterdam, 1994.
14. Nilsson, R., Lindblad, T., and Andersson, A., *J. Catal.* **148**, 501 (1994).
15. Barbaro, A., Larrondo, S., Duhalde, S., and Amadeo, N., *Appl. Catal. A* **193**, 277 (2000).
16. Grasselli, R. K., *Catal. Today* **49,** 141 (1999).
17. Grasselli, R. K., *in* "Handbook of Heterogeneous Catalysis: Ammoxidation (G. Ertl, H. Knoezinger, J. Weitkamp, Eds.), Vol. 5, p. 2302. Wiley, New York, 1997.
18. Birchall, T., and Sleigth, A. W., *Inorg. Chem.* **15**(4), 868 (1976).
19. Centi, G., and Mazzoli, P., *Catal. Today* **28**, 351 (1996).
20. Centi, G., Perathoner, S., and Trifirò, F., *Appl. Catal. A* **157**, 143 (1997).
21. Hansen, S., Ståhl, K., Nilsson, R., and Andersson, A., *J. Solid State Chem.* **102**, 340 (1993).
22. Centi, G., and Trifiró, F., *Catal. Rev. Sci. Eng.* **28**, 165 (1986).
23. Berry, F. J., Holden, J. G., and Loretto, M. H., *J. Chem. Soc. Faraday Trans.* **83**, 615 (1987).
24. Anderson, A. B., *J. Chem. Phys.* **62**, 1187 (1975).
25. Landrum, G.,"Yet Another Extended Hückel Molecular Orbital Package (YAEHMOP)," Cornell University, 1997. [YAEHMOP is freely available on the World Wide Web at http://overlap.chem.cornell.edu:8080/yaehmop.html]
26. Sambeth, J., Juan, A., Gambaro, L., and Thomas, H., *J. Mol. Catal.* **118**, 283 (1997).
27. Irigoyen, B., Castellani, N., and Juan, A., *J. Mol. Catal.* **129**, 297 (1998).
28. Irigoyen, B., Juan, A., and Castellani, N., *J. Catal.* **190**, 1, 14 (2000).
29. Berry, F. J., Smart, L. E., and Duhalde, S., *Polyhedron* **15**, 4, 651 (1996).
30. Callahan, J. L., and Grasselli, R. K., *AIChE J.* **9**, 755 (1963).
31. Keidel, F. A., and Bauet, S. H., *J. Chem. Phys.* **26**, N6 (1956).
32. Morrison, R. T., and Boyd, R. N., "Organic Chemistry." Allyn and Bacon, New York, 1994.
33. Berry, F., Brett, M., and Patterson, W. R., *J. Chem. Soc. Dalton Trans.* 13 (1983).
34. Grzybowska-Swierkosz, B., *Topics in Catal.* **11/12**, 23 (2000).
35. Busca, G., Centi, G., Trifirò, F., and Lorenzelli, V., *J. Phys. Chem.* **90**, 1337 (1986).
36. Busca, G., Centi, G., and Trifirò, F., *Appl. Catal.* **25**, 265 (1986).
37. Busca, G., Lorenzelli, V., Olivieri, G., and Ramis, G., *Stud. Surf. Sci. Catal.* **82**, 253 (1994).
38. Finocchio, E., Ramis, G., Busca, G., Lorenzelli, V., and Willey, R. J., *Catal. Today* **28**, 381 (1996).
39. Weber, R. S., *J. Phys. Chem.* **98**, 2999 (1994).
40. Oyama, S. T., Desikan, A. N., and Zhang, W., *in* "Catalytic Selective Oxidations" (S. T. Oyama and J. W. Hightower, Eds.), ACS Symposium Series, Vol. 523, p. 16. Am. Chem. Soc., Washington, DC, 1993.
41. Mattheiss, L. F., *Phys. Rev. B* **13**, 2433 (1976).

42. Grunes, L., Leopman, R. D., Wilker, C. N., Hoffmann, R., and Kunz, A. B., *Phys. Rev. B* **25**, 7157 (1982).
43. Hoffmann, R., "Solids and Surfaces: A Chemist's View of Bonding in Extended Structures." Wiley–VCH, New York, 1988.
44. Burdett, J. K., and Hughbanks, T., *Inorg. Chem*. **24**, 1741 (1985).
45. Burdett, J. K., *Inorg. Chem*. **24**, 2244 (1985).
46. Henrich, V. E., *Rep. Prog. Phys.* **48**, 1481 (1985).
47. Halet, J. F., and Hoffmann, R., *J. Am. Chem. Soc.* **111**, 3548 (1989).
48. Hoffmann, R., *J. Chem. Phys.* **39**, 1397 (1963).
49. Kubácek, P., Hoffmann, R., and Havlas, Z., *Organometallics* **1**, 180 (1982).
50. Hughbanks, T., Hoffmann, R., Whangbo, M. -H., Stewart, K. R., Eisenstein, O., and Canadell, E., *J. Am. Chem. Soc.* **104**, 3876 (1982).
51. Minot, C., and Gallezott, P., *J. Catal.* **123**, 341 (1990).